NewsStand, Inc. - Today's Way To Read Publications--Digitally - Microsoft Internet Explorer



17. Milkovich, S. M. & Head, J. W. III North polar cap of Mars: Polar layered deposit characterization and identification of a fundamental climate signal. *J. Geophys. Res.* **110,** E01005, doi:10.1029/2004JE002349 (2005).
18. Tanaka, K. L. The stratigraphy of Mars. *J. Geophys. Res.* **91,** E139–E158 (1986).
19. Hartmann, W. K. & Neukum, G. Cratering chronology and the evolution of Mars. *Space Sci. Rev.* **96,** 165–194 (2001).
20. Laskar, J. *et al.* Long term evolution and chaotic diffusion of the insolation quantities of Mars. *Icarus* **170,** 343–364 (2004).
21. Parker, T. J., Saunders, R. S. & Schneeberger, D. M. Transitional morphology in west Deuteronilus Mensae, Mars: Implications for modification of the lowland/upland boundary. *Icarus* **82,** 111–145 (1989).
22. Baker, V. R. *et al.* Ancient oceans, ice sheets, and the hydrological cycle on Mars. *Nature* **352,** 589–594 (1991).
23. Wyatt, M. B., McSween, H. Y. Jr, Tanaka, K. L. & Head, J. W. III. Global geologic context for rock types and surface alteration on Mars. *Geology* **32,** 645–648 (2004).
24. Mustard, J. F., Cooper, C. D. & Rifkin, M. K. Evidence for recent climate change on Mars from the identification of youthful near-surface ground ice. *Nature* **412,** 411–414 (2001).
25. Robertson, A. & Ocean Drilling Program Leg 160 Scientific Party. Mud volcanism on the Mediterranean Ridge: Initial results of Ocean Drilling Program Leg 160. *Geology* **24,** 239–242 (1996).
26. Mellon, M. T. & Jakosky, B. M. The distribution and behaviour of Martian ground ice during past and present epochs. *J. Geophys. Res.* **100,** 11781–11799 (1995).
27. Fishbaugh, K. E. Characterization of Martian north polar geologic units using Mars Odyssey THEMIS data. *Lunar Planet Sci. Conf.* [CD-ROM] XXXVI, Abstr. no. 1335 (2005).
28. Rahmstorf, S. Timing of abrupt climate change: A precise clock. *Geophys. Res. Lett.* **30,** doi:10.1029/2003GL017115 (2003).

**Acknowledgements** I acknowledge discussions and other assistance from S. Byrne, K. Fishbaugh, E. Kolb, K. Herkenhoff, A. Rodriguez, J. Skinner and T. Hare. This work was supported by NASA.

**Author Information** Reprints and permissions information is available at npg.nature.com/reprintsandpermissions. The author declares no competing financial interests. Correspondence and requests for materials should be addressed to the author (ktanaka@usgs.gov).





LETTERS

# Coherent signal amplification in bistable nanomechanical oscillators by stochastic resonance

Robert L. Badzey[1] & Pritiraj Mohanty[1]

**Stochastic resonance[1,2] is a counterintuitive concept: the addition of noise to a noisy system induces coherent amplification of its response. First suggested as a mechanism for the cyclic recurrence of ice ages, stochastic resonance has been seen in a wide variety of macroscopic physical systems: bistable ring lasers[3], superconducting quantum interference devices[4,5] (SQUIDs), magnetoelastic ribbons[6] and neurophysiological systems such as the receptors in crickets[7] and crayfish[8]. Although fundamentally important as a mechanism of coherent signal amplification, stochastic resonance has yet to be observed in nanoscale systems. Here we report the observation of stochastic resonance in bistable nanomechanical silicon oscillators. Our nanomechanical systems consist of beams that are clamped at each end and driven into transverse oscillation with the use of a radiofrequency source. Modulation of the source induces controllable switching of the beams between two stable, distinct states. We observe that the addition of white noise causes a marked amplification of the signal strength. Stochastic resonance in nanomechanical systems could have a function in the realization of controllable high-speed nanomechanical memory cells, and paves the way for exploring macroscopic quantum coherence and tunnelling.**

The conditions for a system to exhibit stochastic resonance are well known and fairly robust. First among these is an energy threshold. Second, there needs to be an applied subthreshold modulation, which causes the system to cross the threshold. And last, there needs to be a source of noise. One of the classic examples of a system that undergoes stochastic resonance is that of a particle in a double-well potential. With no modulation, the particle will undergo a transition between the two wells with the Kramers rate, $T_K \propto e^{-\Delta V/D}$, where $\Delta V$ is the depth of each well and $D$ is the strength of temperature-induced noise. With the addition of external periodic modulation there is an interaction between the modulation and the noise, resulting in a resonance in the signal-to-noise ratio (SNR), which is defined[2] as

$$\mathrm{SNR} = 2\left[\lim_{\Delta\omega\to 0}\int_{\Omega-\Delta\omega}^{\Omega+\Delta\omega} S(\omega)\mathrm{d}\omega\right]/N(\Omega) = \frac{S(\Omega)}{N(\Omega)} \qquad (1)$$

where $S(\Omega)$ is the height of the power spectrum peak at the modulation frequency $\Omega$ and $N(\Omega)$ is the spectral background.

It is well known that, with suitably strong driving, the linear response of a damped, driven harmonic oscillator undergoes a transition to that of a nonlinear bistable system, which is the famous Euler instability. The equation of motion is described by the Duffing equation with driving force $F$ and driving amplitude $\omega$:

$$\ddot{x} + \gamma\dot{x} + kx \pm k_3x^3 = F\cos\omega t \qquad (2)$$

Here, $k$ and $k_3$ are the linear and nonlinear spring constants, respectively, and $\gamma$ is the damping coefficient describing the dissipation of the oscillator. The sign of the $k_3$ term changes depending on whether the oscillator is under compressive (positive $k_3$) or tensile (negative $k_3$) strain. The presence of the cubic term in the equation of motion naturally leads to a term of fourth order in the beam potential, which implies that the oscillator now demonstrates bistability[9–11]. It is important to note that, regardless of the sign of the nonlinear term, both instances will result in a bistable oscillator. This is clear from the amplitude response of the Duffing oscillator: when looking at the amplitude response as a function of frequency, one finds that the oscillator no longer displays the symmetric lorentzian line shape characteristic of a damped, driven, linear harmonic oscillator. Rather, there is a sharp bend in the peak that creates a region of frequency space in which the oscillator is multi-valued. If the oscillator is softening, the bend occurs to the left of the location of the linear peak; similarly, the bend is on the right for a hardening spring. The signature of a system in nonlinear response is a hysteresis defined by sweeping the driving frequency forwards and backwards through the bistable region. For instance, in the compressive case, as the frequency is increased, the response will follow state 1 until reaching a point of instability, whereupon it will drop sharply to state 2. A downward sweep will produce the opposite effect, defining a region in which the beam is bistable; these situations are reversed for a softening spring. Excitation at a single frequency within this region allows one to access either of the two bistable states by the addition of a suitable modulation[12]. In each case, bistable behaviour holds only for driving frequencies near resonance.

Strictly speaking, the above description is that of a point particle in a double-well potential with no additional modulation or noise terms. For a spatially extended system such as a doubly clamped beam or string under additional modulation and external noise, the more appropriate description is the Landau–Ginzburg equation, in which the field variable $\Phi(x)$ replaces the position variable $x$:

$$\frac{\mathrm{d}\Phi(x)}{\mathrm{d}t} = m\Phi(x) - \Phi^3(x) + \kappa\frac{\mathrm{d}^2\Phi(x)}{\mathrm{d}x^2} + F_{\mathrm{mod}}\cos\Omega t + \eta(x,t) \qquad (3)$$

Here $\Omega$ is the modulation frequency and $\eta(x,t)$ is the added noise term. In their seminal paper, Benzi *et al.*[13] predicted the emergence of stochastic resonance in a doubly clamped beam or string described by the Landau–Ginzburg equation with Von Neumann boundary conditions, $\mathrm{d}\Phi(0)/\mathrm{d}x = \mathrm{d}\Phi(L)/\mathrm{d}x = 0$. In addition to the two stable homogeneous solutions corresponding to the occupation of either well, there also exists a class of instanton solutions which imply that in the presence of noise the string can undergo a transition between the two wells. In this case, the string collective coordinate $u = (1/L)\int_0^L \Phi(x)\mathrm{d}x$ synchronizes with the modulation within a certain range of noise powers. The behaviour of the collective coordinate as a particle in a double-well potential therefore completes the projection of the doubly clamped beam into the canonical single-particle picture described above.

We have fabricated two doubly clamped nanomechanical beams from single-crystal silicon with e-beam lithography and dry etching.

[1]Department of Physics, Boston University, 590 Commonwealth Avenue, Boston, Massachusetts 02215, USA.



NATURE 10/13/2005 Section: Letters to Nature Page: 994/995
Интернет
пуск The Bat! NewsStand, I... NewsStand, I... Adobe Acrob... EN 9:50

NewsStand, Inc. - Today's Way To Read Publications--Digitally - Microsoft Internet Explorer



Frequency sweeps with increasing drive amplitude show a marked evolution from the familiar lorentzian response into a shifted response with a sharp drop and marked hysteresis. We perform forward and reverse frequency sweeps with large driving amplitudes to confirm and record the onset of nonlinear and bistable behaviour. We then drive each bridge at a single frequency within its unique bistable frequency region to access both bistable states by means of the addition of a modulation signal of suitable strength. Our samples are driven with the well-known magnetomotive technique[14]; Fig. 1 shows a diagram of the circuit used to drive the bistable oscillator and add white noise.

Beam 1 is cooled to 300 mK and driven nonlinear with $A_{drive} = 4.0$ dBm. The modulation is made too weak (−5.5 dBm) to induce switching, and the noise is swept from −71 dBm (~79 pW) to −41 dBm (~79 nW). At each noise power, a time series is taken to monitor the oscillator response. Figure 2A shows selected time series at different noise powers, with their associated power spectra. After calculating the SNR, the data are combined and represented in Fig. 2B. The resonance is clear and marked, with a sharp increase in SNR at ~18 nW. These noise powers are those coming from the source rather than the actual power incident on the sample.

It has been shown[15] that the temperature of the beam is a viable source of noise, causing a decrease in switching fidelity and increase in state noise at temperatures below 1 K. There should therefore be a temperature or range of temperatures above 1 K where we would actually see an increase in the SNR. Beam 2 is disconnected from the noise source. In this case, the beam achieves a nonlinear response with a smaller driving amplitude (1.0 dBm), whereas the amplitude necessary for switching is much greater (>16.5 dBm). Because the modulation power is so large, the electrical signal actually shows up in our lock-in technique, as can be seen in Fig. 3A. Again, the left-hand side shows segments from the time series at each temperature

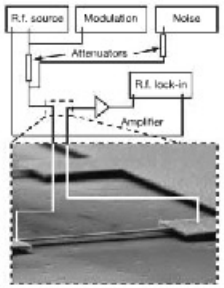


**Figure 1 | Diagram of measurement circuit.** The circuit serves to excite the nonlinear motion of the beam, modulate the switching, and add in noise to achieve stochastic resonance. The radiofrequency (r.f.) source is a Rohde & Schwarz function generator, operating at a frequency within the bistable region (either 23.4973 or 20.8343 MHz, depending on the beam), at a driving amplitude of 4.0 dBm (beam 1) or 1.0 dBm (beam 2). The modulation is produced by an HP 3325 synthesizer, with an amplitude of −5.5 dBm (beam 1) or 16.5 dBm (beam 2). In both cases the modulation is a square wave with a frequency of 0.05 Hz. The white-noise source is an HP 33220 synthesizer, capable of creating white noise in a band between 0 and 15 MHz. For the temperature sweep (beam 2) the noise source was disconnected. The attenuator is an 8 kΩ resistor; the noise source has a separate 30 dB attenuator at the source output. Our beams are 7–8 μm × 300 nm × 200 nm in dimension, and are placed in a $^3$He cryostat (300 mK to 4 K) at the centre of a 9-T superconducting solenoid magnet.

(with the modulation amplitude highlighted in grey), whereas the right-hand side shows the power spectra obtained by fast Fourier transform (FFT). It is immediately apparent that the switching is much noisier than that of beam 1, even when one takes into account the background effect of the modulation. Full switching is never really achieved, even for the most responsive time series.

The difficulty in inducing switching behaviour can be understood by considering the symmetry of the double-well potential. The response of beam 1 led to the conclusion that the potential is very nearly symmetric. However, it rapidly became apparent that this was not true of beam 2. This is especially evident when looking at

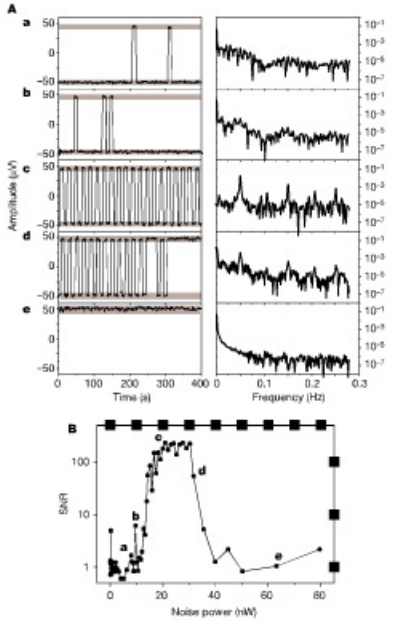


**Figure 2 | Re-emergence of switching behaviour as a function of added white noise on beam 1 ($f_{drive}$ = 23.4973 MHz).** **A**, The left-hand graphs show selected beam responses as a function of added noise power, with lower powers at the top. The grey bands represent the noise of each state, including contributions to the electrical signal from the modulation itself. There is no response until −10 nW of power is introduced (**a**), when a few sporadic switches are seen. As expected, the power spectrum of the response shows no dominant spectral components. With increasing noise power, we observe an increase of switch events, as shown in **b** (13 nW) and **c** (27 nW). Finally, as the noise is increased still further, the switches begin to die out (**d**, 32 nW) until a regime of no switching occurs (**e**, 63 nW). The right-hand column of plots shows the FFT of the data in the left column. As can be expected, there are sharp peaks at 0.05 Hz and all odd harmonics thereof, as befits the square-wave response of the switch. **B**, Each individual scan was processed to obtain the SNR for each noise power. The letters **a**–**e** correspond to the scans in A.





Fig. 3A,b. At each impulse from the modulation there is a sharp spike up to the upper state, which immediately decays down to the lower state; this is an indication that the potential of the bridge is asymmetric. The occurrence of incoherent switches down to the lower state is so prevalent that even when the SNR is maximized, the switching is not truly coherent. This is in sharp contrast to the very clean, symmetric behaviour shown by beam 1. In addition, a look at the power spectra from bridge 2 reveals the presence of even-order harmonics, a sure signature of an asymmetric potential[16,17]. The spring coefficients $k_1$ and $k_3$ change with temperature, which might affect the symmetry and even the shape of the potential. Such a change is manifested by a shift of the resonance frequency of the

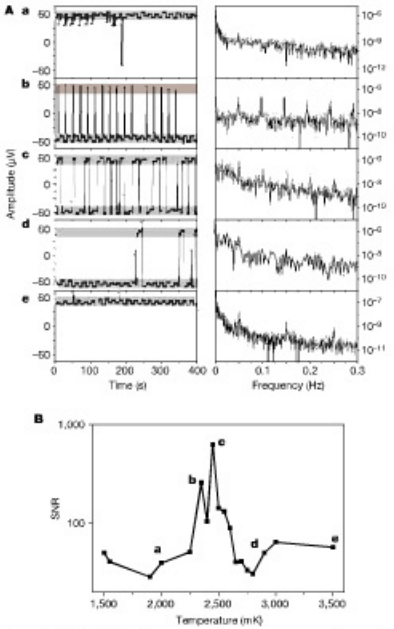


**Figure 3 | Switching behaviour as a function of temperature on beam 2 ($f_{drive}$ = 20.8348 MHz).** **A**, As the temperature is increased, switching behaviour again re-emerges. The modulation is seen in all graphs. Again, the right-hand column shows the FFT of the left-hand column, demonstrating the coherence of the signal as the switches re-emerge. The frequency spectrum shows many more peaks than one would naively expect from a simple square-wave response. This is at least partly due to the increased number of incoherent switches evidenced in this beam. **a**, 2,000 mK; **b**, 2,450 mK; **c**, 2,600 mK; **d**, 2,800 mK; **e**, 3,500 mK. **B**, The SNR was obtained from each individual scan, with a clear resonance occurring at −2,600 mK (2.6 K). The line simply connects each individual temperature point, with no fit involved or implied. In contrast to the very broad resonance seen with noise power, this peak is quite sharp and dies off very quickly. This is not unexpected, because the sweep in temperature is much coarser than that used with noise.

beam with a change in temperature, which is proportional to the sound velocity $v = \sqrt{(E/\rho)}$, where $E$ is the Young modulus and $\rho$ is the material density. As the temperature is reduced, the modulus is increased, leading to a subsequent increase in the resonance frequency. However, we found that such frequency shifts were on the order of less than $10^{-4}$ within the temperature range we employed during these experiments.

Another important question is the effect of temperature on the dissipation coefficient $\gamma$. Should the effect be non-negligible, there exists a multiplicative noise term in the Duffing equation. This is in sharp contrast to the purely additive noise of the classic theory of stochastic resonance. The dissipation is most easily quantified by measuring the quality factor $Q$ of the oscillator as a function of temperature. Our measurements of this quantity indicate that $Q$ can change by as much as 10% over the temperature range 2–3 K.

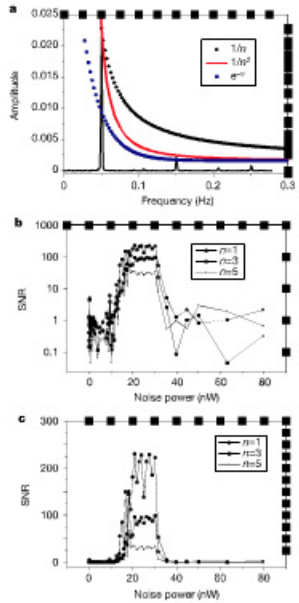


**Figure 4 | Behaviour of higher harmonics.** **a**, The power spectrum from a representative time series, showing the presence of spectral peaks at the odd harmonics of the modulation frequency. This is one of the hallmarks of the square wave drive and response; a sine wave would have a single fundamental peak at the modulation frequency. The three curves represent fits of the peak height versus $n$, the harmonic number: black diamonds, $1/n$; red line, $1/n^2$; blue circles, $e^{-n}$. As expected, the peak height varies as $1/n^2$. **b**, Comparison of the SNR for the higher harmonics with the fundamental. Filled squares, $n = 1$; open circles, $n = 3$; crosses, $n = 5$. For comparison, all three graphs are plotted at the same scale as Fig. 3b. **c**, The SNR for each frequency is plotted again, with the $y$ axis plotted on a linear, rather than a logarithmic, scale, to emphasize the difference in SNR for each frequency. Symbols as in **b**.



NATURE 10/13/2005 Section: Letters to Nature Page: 996/997
Интернет
пуск The Bat! NewsStand, I... NewsStand, I... 1310 3.pdf EN 9:51

NewsStand, Inc. - Today's Way To Read Publications--Digitally - Microsoft Internet Explorer



Although this is not a huge effect, it can certainly have an impact on the system noise, and is definitely worth exploring in more detail. The topic of stochastic resonance has been broached in the literature[18,19], but this provides an avenue for continued research (A. Bulsara, personal communication).

Again, an analysis of each power spectrum produces the SNR value, and these points are compiled to create Fig. 3B. The peak of SNR is much sharper than that seen in beam 1. This might at least in part be due to the rather coarse sweep, when looked at from the perspective of input noise. The apparent increase in SNR at higher temperatures (>3,000 mK) is somewhat misleading. This is due to the still-present signal from the modulation, which produces a peak in the power spectrum and is not due to actual switching between the two bistable states. Filtering the data to excise the effect of modulation would undoubtedly produce a cleaner power spectrum, but the data are presented raw to underscore the presence of stochastic resonance in a system that is less than optimal in potential symmetry and background noise.

In sharp contrast to most other systems investigated for stochastic resonance, we use a square-wave modulation, as opposed to the canonical sine wave. This is an experimental consideration, because we found that switching was much more easily achieved with a square wave. Although a seemingly minor technical difference, there are some important ramifications of the use of this type of modulation. Among these, the modulation signal can be decomposed into the form

$$S_{mod} = \sum_{n=1}^{\infty} a_n \cos n\Omega t + b_n \sin n\Omega t \qquad (4)$$

Here $S_{mod}$ is the input signal, $n$ is the harmonic number, and $\Omega$ is the modulation angular frequency. For a linear response system that follows ref. 20 this does not significantly alter the SNR behaviour; the ratio is still dominated by the fundamental frequency. However, in the presence of a square wave there should be amplifications at other harmonics (M. Grifoni, personal communication) of the fundamental and they should be related to the fundamental SNR as $\mathrm{SNR}(\Omega)/\mathrm{SNR}(n\Omega) = n^2$. For a square wave, only the odd harmonics should be present. Figure 4a shows a representative power spectrum from beam 1, plotted on a linear scale to emphasize the peak height. As can be seen, the peak heights scale most closely as $1/n^2$. For a flat background noise spectrum, peak height and SNR are the same quantity. In addition, Fig. 4b, c shows the SNRs from the fundamental and the first two odd harmonics. Figure 4b shows all three on the same scale as Fig. 2B, whereas Fig. 4c shows them plotted on a linear scale to emphasize the difference in the SNR. Theoretical investigations in this area are few[21,22] but we hope that in the light of this experiment more work might be done making this distinction.

It is typical that after exceeding the maximum noise needed to induce stochastic resonance, the time scan would be characterized by a very noisy response dominated by incoherent switches caused by the large noise power. In contrast, both of these systems show no switching at all when reaching the upper limit of noise power, instead settling on one state. As mentioned above, this is not a system with a static bistability—rather, its bistable and nonlinear behaviour is induced by the presence of a strong drive. This drive and the hysteresis it creates impart a certain amount of rigidity to the system, making switching between the two states difficult. In comparison with the size of the signal required to both form the bistable two-state system and to achieve full switching in the absence of noise (~1–10 dBm), the maximum amount of noise induced either externally or by temperature is orders of magnitude smaller. This is certainly a topic worthy of future investigation, because this dynamic bistability is one of the fundamental aspects that departs from the canonical stochastic resonance model.

The presence of stochastic resonance in these systems is exciting not only for its inherent physical interest but also because it brings up the possibility of using stochastic resonance as a means of enhancing signal processing. If the nanomechanical memory element does indeed turn out to be a viable technological innovation, stochastic resonance may very well be one of the mechanisms that permit its everyday use. Even though our system is manifestly classical, it is closely related to at least one quantum-mechanical system (the macroscopic quantum harmonic oscillator[23]). The demonstration of stochastic resonance in this system enables the exploration of stochastic resonance in a quantum-mechanical context on a system that is at the very forefront of quantum logic, quantum control and quantum computation.

**Received 2 June; accepted 11 August 2005.**


1. Benzi, R., Sutera, A., Parisi, G. & Vulpiani, A. A theory of stochastic resonance in climatic change. *J. Appl. Math.* **43**, 565–578 (1983).
2. Gammaitoni, L., Hänggi, P., Jung, P. & Marchesoni, F. Stochastic resonance. *Rev. Mod. Phys.* **70**, 223–287 (1998).
3. McNamara, B., Wiesenfeld, K. & Roy, R. Observation of stochastic resonance in a ring laser. *Phys. Rev. Lett.* **60**, 2626–2629 (1988).
4. Hibbs, A. D. *et al.* Stochastic resonance in a superconducting loop with a Josephson junction. *J. Appl. Phys.* **77**, 2582–2590 (1995).
5. Rouse, R., Han, S. & Lukens, J. E. Flux amplification using stochastic superconducting quantum interference devices. *Appl. Phys. Lett.* **66**, 108–110 (1995).
6. Spano, M. L., Wun-Fogle, M. & Ditto, W. L. Experimental observation of stochastic resonance in a magnetoelastic ribbon. *Phys. Rev. A* **46**, R5253–R5256 (1992).
7. Levin, J. E. & Miller, J. P. Broadband neural encoding in the cricket cercal sensory system enhanced by stochastic resonance. *Nature* **380**, 165–168 (1996).
8. Douglass, J. K., Wilkens, L., Pantazelou, E. & Moss, F. Noise enhancement of information transfer in crayfish mechanoreceptors by stochastic resonance. *Nature* **365**, 337–340 (1993).
9. Carr, S. M., Lawrence, W. E. & Wybourne, M. N. Accessibility of quantum effects in mesomechanical systems. *Phys. Rev. B* **64**, 220101 (2001).
10. Nayfeh, A. H. & Mook, D. T. *Nonlinear Oscillations* (Wiley, New York, 1979).
11. Weaver, W., Timoshenko, S. P. & Young, D. H. *Vibration Problems in Engineering* (Wiley, New York, 1990).
12. Badzey, R. L., Zolfagharkhani, G., Gaidarzhy, A. & Mohanty, P. A controllable nanomechanical memory element. *Appl. Phys. Lett.* **85**, 3587–3589 (2004).
13. Benzi, R., Sutera, A. & Vulpiani, A. Stochastic resonance in the Landau–Ginzburg equation. *J. Phys. A* **18**, 2239–2245 (1985).
14. Greywall, D. S., Yurke, B., Busch, P. A., Pargellis, A. N. & Willett, R. L. Evading amplifier noise in nonlinear oscillators. *Phys. Rev. Lett.* **72**, 2992–2995 (1994).
15. Badzey, R. L., Zolfagharkhani, G., Gaidarzhy, A. & Mohanty, P. Temperature dependence of a nanomechanical switch. *Appl. Phys. Lett.* **86**, 023106 (2005).
16. Inchiosa, M. E., Bulsara, A. R. & Gammaitoni, L. Higher-order resonant behaviour in asymmetric nonlinear stochastic systems. *Phys. Rev. E* **55**, 4049–4056 (1997).
17. Inchiosa, M. E. & Bulsara, A. R. dc signal detection via dynamical asymmetry in a nonlinear device. *Phys. Rev. E* **58**, 115–127 (1998).
18. Bulsara, A., Jacobs, E. W., Zhou, T., Moss, F. & Kiss, L. Stochastic resonance in a single neuron model—theory and analog simulation. *J. Theor. Biol.* **152**, 531–555 (1991).
19. Gammaitoni, L., Marchesoni, F., Menichellasaetta, E. & Santucci, S. Multiplicative stochastic resonance. *Phys. Rev. E* **49**, 4878–4881 (1994).
20. McNamara, B. & Wiesenfeld, K. Theory of stochastic resonance. *Phys. Rev. A* **39**, 4854–4869 (1989).
21. Morillo, M. & Gomez-Ordoñez, J. Amplification and distortion of a periodic rectangular driving signal by a noisy bistable system. *Phys. Rev. E* **51**, 999–1003 (1995).
22. Casado-Pascual, J., Gomez-Ordoñez, J. & Morillo, M. Nonlinear stochastic resonance with subthreshold rectangular pulses. *Phys. Rev. E* **69**, 067101 (2004).
23. Gaidarzhy, A., Zolfagharkhani, G., Badzey, R. & Mohanty, P. Evidence for quantized displacement in macroscopic nanomechanical oscillators. *Phys. Rev. Lett.* **94**, 030402 (2005).


**Acknowledgements** We acknowledge the Nanoscale Exploratory Research (NER) program of the National Science Foundation and the DOD/ARL for the financial support of this research.

**Author Information** Reprints and permissions information is available at npg.nature.com/reprintsandpermissions. The authors declare no competing financial interests. Correspondence and requests for materials should be addressed to P.M. (mohanty@physics.bu.edu).





LETTERS

# Synthesis and properties of crosslinked recombinant pro-resilin

Christopher M. Elvin[1], Andrew G. Carr[1], Mickey G. Huson[2], Jane M. Maxwell[2], Roger D. Pearson[1], Tony Vuocolo[1], Nancy E. Liyou[1], Darren C. C. Wong[1,3], David J. Merritt[3] & Nicholas E. Dixon[4]

**Resilin is a member of a family of elastic proteins that includes elastin, as well as gluten, gliadin, abductin and spider silks. Resilin is found in specialized regions of the cuticle of most insects, providing low stiffness, high strain and efficient energy storage[1,2]; it is best known for its roles in insect flight[3,4] and the remarkable jumping ability of fleas[5,6] and spittle bugs[7]. Previously, the *Drosophila melanogaster* CG15920 gene was tentatively identified as one encoding a resilin-like protein[8,9] (pro-resilin). Here we report the cloning and expression of the first exon of the *Drosophila* CG15920 gene as a soluble protein in *Escherichia coli*. We show that this recombinant protein can be cast into a rubber-like biomaterial by rapid photochemical crosslinking. This observation validates the role of the putative elastic repeat motif in resilin function. The resilience (recovery after deformation) of crosslinked recombinant resilin was found to exceed that of unfilled synthetic polybutadiene, a high resilience rubber. We believe that our work will greatly facilitate structural investigations into the functional properties of resilin and shed light on more general aspects of the structure of elastomeric proteins. In addition, the ability to rapidly cast samples of this biomaterial may enable its use *in situ* for both industrial and biomedical applications.**

The outstanding mechanical properties of resilin were discovered four decades ago during studies of the flight systems of desert locusts and dragonflies[3,10]. Weis-Fogh proposed a model for elasticity in which randomly coiled, crosslinked polypeptide chains underwent a decrease in entropy upon straining[10,11]. The chemical crosslinks in resilin from insect joints and tendons occur between tyrosine residues, generating di- and trityrosine[1,12]. A structural description of the functional properties of the family of elastic proteins has been elusive, but recent studies on elastin[13–15] suggest that its elasticity is due to the extremely dynamic nature of amorphous hydrophobic domains, which form a kinetically free, random-network polymer.

Naturally crosslinked resilin exhibits two outstanding material properties: it has high rubber efficiency (resilience) and a very high fatigue lifetime. Apart from its role in flight and locomotion, it is also used for other insect functions where efficient energy storage and repetitive movement are required—for example, in the sound-producing organs of cicadas[16] and moths[17], as well as in crustaceans[18]. It is also present in some stretchable cuticular structures that do not possess long-range elasticity, including the abdominal wall of physogastric termite queens[19] and in the spermatophore wall of ticks[20].

All elastic proteins contain distinct domains, of which at least one is made up of elastic repeat sequences, and they all contain crosslinks between residues in either the non-elastic or elastic domains[21]. To prepare recombinant resilin, we chose to express the first exon of the *Drosophila* CG15920 gene, which encodes an amino-terminal domain in the native protein comprising 17 copies of the putative elastic repeat motif, GGRPSDSYGAPGGGN (ref. 8). We cloned and expressed this region (which we refer to as rec1-resilin) as a soluble protein in *E. coli* (Fig. 1a, Methods and Supplementary Information, part 1).

To generate solid, crosslinked rec1-resilin, conditions were established for formation of dityrosine crosslinks between soluble proteins to produce very high molecular weight crosslinked polymeric material. Quantitative crosslinking of soluble rec1-resilin was achieved by use of *Arthromyces ramosus* peroxidase, an enzyme known to catalyse dityrosine formation[22]. A solid biomaterial formed only from concentrated (>100 mg ml$^{-1}$) solutions of purified rec1-resilin. This method was of limited value for casting material for physical testing, since the rate of the enzyme-catalysed reaction was uncontrollably fast and the catalase activity of the peroxidase formed oxygen bubbles in the sample. On the other hand, Ru(II)-mediated photo-crosslinking[23] resulted in rapid, quantitative and

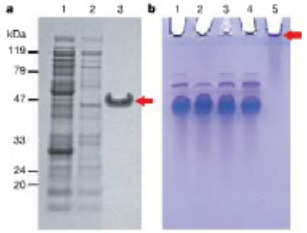


**Figure 1 | Purification and crosslinking of soluble recombinant rec1-resilin. a**, 10% SDS–PAGE of samples from steps in the purification. Lane 1, cleared supernatant from lysed cells; lane 2, flow-through from Q-Sepharose; lane 3, protein eluted from Ni-NTA agarose with a 50–200 mM imidazole gradient (arrow) (see Supplementary Information, part 1.6 for details). **b**, Photo-crosslinking of soluble rec1-resilin analysed on SDS–PAGE. Irradiation (600 W at 15 cm) of a solution of protein (1 mg ml$^{-1}$) containing $[Ru(bpy)_3]^{2+}$ (200 μM) and ammonium persulphate (APS; 10 mM) produces polymerized rec1-resilin which barely enters a 10% SDS–PAGE gel (arrow). Lane 1, with Ru(II) and APS (no light); lane 2, rec1-resilin only; lane 3, with Ru(II) only; lane 4, with APS only; lane 5, with Ru(II) and APS, 20-s irradiation as described in Supplementary Information, part 1.8.

[1]CSIRO Livestock Industries, Queensland Bioscience Precinct, St Lucia 4072, Australia. [2]CSIRO Textile and Fibre Technology, PO Box 21, Geelong 3216, Australia. [3]School of Integrative Biology, University of Queensland, St Lucia 4072, Australia. [4]Research School of Chemistry, Australian National University, Canberra 0200, Australia.



NATURE 10/13/2005 Section: Letters to Nature Page: 998/999
Интернет
пуск The Bat! NewsStand, I... NewsStand, I... 1310 3.pdf EN 9:52